A Lithium-Tantalate Based Acoustic Reflective Delay Line for Chemical Sensing in Water

J.-M Friedt, D. Rabus, L. Arapan, V. Luzet, F. Chérioux
Université de Franche-Comté, CNRS, FEMTO-ST,
F-25000 Besançon, France
jmfriedt@femto-st.fr

N. Nief, S. Dehez, J.R Ordonez-Varela
TotalEnergies
Pau, France
nathalie.nief@totalenergies.com

***Abstract*—Surface acoustic delay lines patterned on lithium tantalate piezoelectric substrate propagating a guided shear wave is demonstrated for direct detection chemical sensing in aqueous solutions with no need for additional microfluidic handling. The high dielectric permittivity substrate prevents excessive losses from capacitive coupling with water when dipping the whole chip, including interdigitated electrodes, in water, while the shear wave only couples with the first few hundred nanometers of the adsorbed layer. A measurement of non-specific protein detection demonstrates the principle.**

***Index Terms*—lithium tantalate, reflective delay line, GPR**

I. Introduction

Thin film-based direct chemical sensing using Surface Acoustic Wave (SAW) transducers has announced promising improved sensitivity over the bulk acoustic wave quartz crystal resonator. Nevertheless, detection limits remain improved in the latter over the former measurement in liquid phase: indeed, the quartz crystal resonator confines energy at the center of the electrodes, allowing an O-ring seal to confine liquid over the sensing area where acoustic energy is maximum and hardly affected by fluidic handling elements, as opposed to the surface acoustic wave geometry that requires confining the liquid over the acoustic cavity between interdigitated transducers (IDTs) or transducer and mirrors, with a significant impact of the fluidic structures over the acoustic path. The tradeoff between efficient sealing requiring a strong bonding of the fluidic handling structure and the weak interaction with the propagating acoustic wave leads to unstable and hardly reproducible ad-hoc solutions [1]–[3].

As long as low permittivity substrates such as quartz are considered, the capacitive short circuit of the electric field in the high permittivity water with a high capacitance favoring currents in the liquid over the piezoelectric substrate will necessarily induce strong insertion losses as long as water is not prevented from reaching the IDTs. In this abstract, we consider the use of lithium tantalate oxide (LTO) for propagating a pure shear wave with low coupling with the surrounding liquid, generated on a high permittivity substrate [4] inducing little losses when the sensor surface is coated with water. We demonstrate sensing capability in an ionic aqueous medium without the need for fluidic confinement.

This work is supported by the French National Research Agency (ANR) under the UNDERGROUND grant ANR-17-CE24-0037 and partial support of the French RENATECH network and its FEMTO-ST technological facility.

II. Lithium tantalate shear wave gravimetric sensitivity

Quartz is most commonly used for SAW sensors for its ability to propagate a pure shear wave confined to the substrate surface by a guiding layer in a Love mode configuration. However the low electromechanical coupling of quartz makes it poorly suited for transmission or reflective delay line due to the high insertion losses or low received power degrading the signal-to-noise ratio (SNR) and hence the detection limit, despite a turnover at room temperature when appropriate crystalline orientations (ST, AT cuts) are selected depending on the temperature coefficient of the guiding layer. Maximum sensitivity is reached when the gradient of the acoustic velocity is maximum as a function of guiding layer thickness, under the condition of limited insertion losses, as assessed experimentally in Fig. 1.

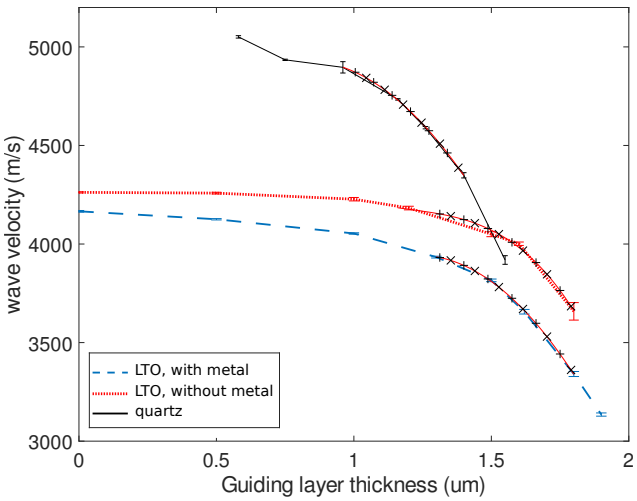

Fig. 1. Acoustic velocity for Love mode propagating on LTO and quartz as a function of polymer Shipley photoresist S18XX guiding layer thickness, with or without metalization on the acoustic path.

Improving the SNR with the selection of a strongly coupled substrate is beneficial, especially in a reflective delay line configuration for wireless measurement. Furthermore, a high permittivity substrate will prevent capacitive coupling of the electric field with the high permittivity ($\varepsilon_r = 80$) water by keeping the electric field in the piezoelectric substrate.

While lithium niobate would be a candidate with its high permittivity ($\varepsilon_r = 20$ to 80 depending on the direction), it is not known to propagate a pure shear wave other than the longitudinal wave with poor gravimetric sensitivity. The selected substrate is hence YXl/42°-LTO or YXl/36°-LTO, with a relative permittivity of $\varepsilon_r = 40$ to 50 depending on the direction but a pseudo-shear wave readily converted to a Love mode with a guiding layer or maintained at close proximity of the substrate surface with a metalization layer slowing the wave velocity. Indeed capacitive coupling, even in the presence of insulating guiding layer preventing resistive coupling to the conducting liquid, between the ε_1 substrate and ε_2 liquid leads to a voltage divider bridge between the capacitors of common area and distance between electrodes so that the division ratio is $\varepsilon_1/(\varepsilon_1+\varepsilon_2)$. When IDTs patterned on quartz with $\varepsilon_1 \simeq 5$ are exposed from air ($\varepsilon_2 \simeq 1$) to water, the coupling to the piezoelectric substrate drops from $5/6$ to $5/85$ or 14-fold, i.e. 23 dB. On the opposite when IDTs on LTO with $\varepsilon_1 \simeq 40$, the same procedure leads to a voltage drop of a factor $(40/41)/(40/120) \simeq 3$ or 9 dB. These quantities match experimental observations.

III. Delay Line Design and Realization

A transmission delay line has been fabricated on LTO exhibiting an insertion loss of 11 dB with the optimized guiding layer thickness confining a Love mode on the substrate surface, a favorable outcome with respect to a quartz delay line typically exhibiting insertion losses in the 18 dB range (Fig. 2) but with the latter dramatically increasing when exposed to water. Selecting an arbitrary threshold on insertion losses of 25 dB for high SNR measurement, a quartz substrate is unable to meet the requirement when exposed to water whereas LTO remains at a level of $11+9=20$ dB insertion losses when dipped in water. For these considerations on transmission delay line designs, a reflective delay line design is considered as needed for passive, wireless sensing.

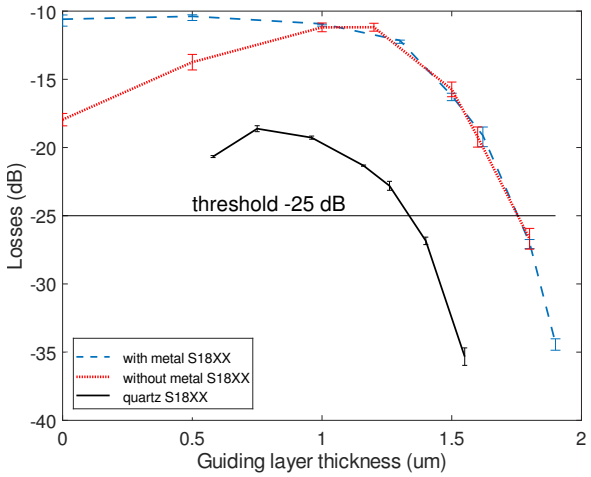

Fig. 2. Acoustic losses of quartz and LTO devices, the latter coated with a Shipley S18XX polymer guiding layer propagating a Love mode either on metalized areas between IDT and mirror or without metalization.

On the opposite, as shown in the frequency domain response (top) and time domain response (bottom) generated as the magnitude of the inverse Fourier transform of the frequency domain response, insertion losses of the time-domain echoes of the LTO delay line exhibit less than 3 dB drop when dipped in deionized water with no protection whatsoever on the acoustic path, IDT or wire bonding (Fig. 3). The frequency domain range is determined by the IDT mechanical period for the center frequency and piezoelectric substrate electromechanical coupling coefficient for the span, while the number of collected samples in the frequency and hence in the time domain is determined by the longest echo delay. Indeed with a 100 MHz center frequency and a 20 MHz span designed to be compatible with commercial, off the shelf Ground Penetrating RADAR (GPR [5]) for passive wireless subsurface pollutant detection, the timestep after inverse Fourier transform is $1000/20 = 50$ ns and collecting 100 samples is sufficient to span the 0 to 5 μs time-domain range determined by the geometric distance of the mirror furthest from the IDT and the acoustic velocity.

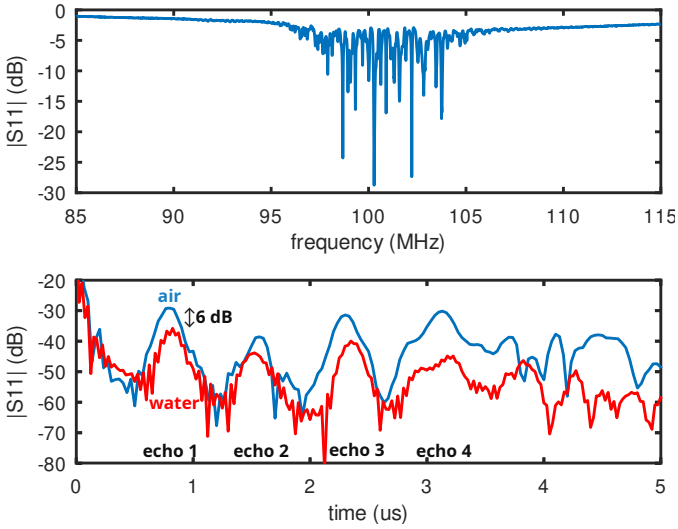

Fig. 3. Top: frequency domain response of the reflective delay line designed with four echoes. Bottom: inverse Fourier transform of the frequency-domain response to recover the time-domain response, with the 4 echoes clearly seen at $N \times 0,8$ μs, $N \in [1:4]$ and 0.8 μs selected as a tradeoff between getting rid of Ground Penetrating RADAR clutter in the first 0.8 μs and limiting the maximum delay and hence path length to 5 μs. In the time domain curve, the blue curve was collected in air and the red curve while dipping the sensor in deionized water with no fluidic protection on the acoustic path, the IDT or the wire bonding, exhibiting less than 6 dB loss between the two conditions.

Most interestingly for wireless sensing applications, the transmission delay line has been extended to a reflective delay line architecture, replacing the second IDT with Bragg mirrors with lengths tuned to allow for two mirrors on both sides of the transducer, hence leading to a differential measurement on a single device when propagation delays introduced by the mirrors are different. Indeed with local chemical functionalization between each mirror, the contribution of sensor range to the interrogation (RADAR) unit, temperature and interfering chemical compound can be subtracted by differential analysis.

Various geometries of mirrors have been investigated, either in an acoustic wave reflective behavior where the acoustic velocity mismatch between free space and metalized space leads to mechanical reflection of the wave and constructive interference back towards the IDT in a Bragg mirror geometry, or in a re-emission geometry where the current generated in the mirror itself polarizes the substrate to create a new acoustic wave at the mirror location. In the former case all electrodes are short circuited or floating, whereas in the latter the electrodes are connected in an IDT geometry. In the latter case, either apodized or uniformly weighted (constant length) interdigitated transducers were patterned on the piezoelectric substrate, in all cases with a short length of electrode on the bus to avoid transverse modes in the strongly coupled piezoelectric substrate. Fig. 4 provides an overview of the mask layout with all experiments triplicated under the same geometry (three measurement channels with four mirrors each), with each chip implementing a different geometry as just explained.

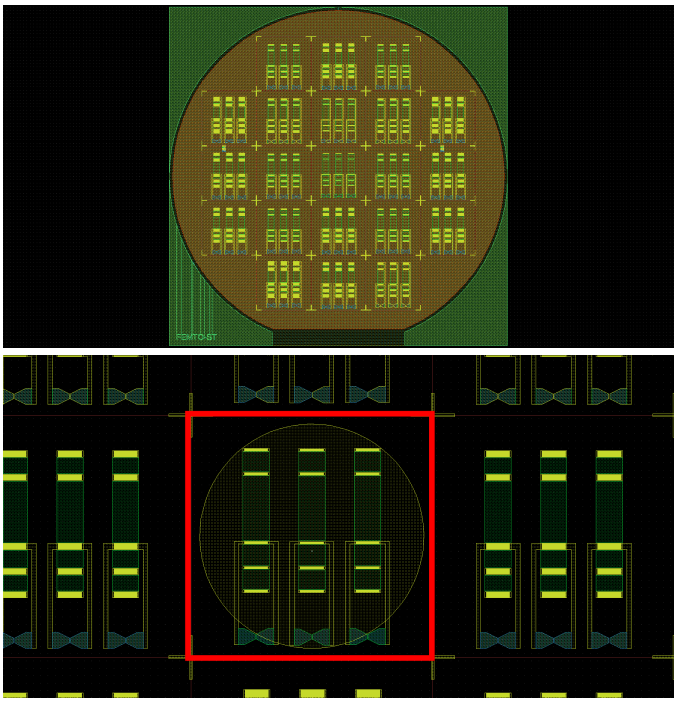

Fig. 4. Top: generally layout of the mask for a 4 inch lithium tantalate wafer. Bottom: zoom on a single sensor chip including three measurement channels for triplicating each measurement sequence, each channel being fitted with four mirrors. It was observed that mirrors evenly distributed at $N \times \tau$ with $N \in [1:4]$ and τ arbitrarily set to 0.8 μs to allow clutter to fade out while limiting acoustic propagation losses led to optimal measurement conditions.

IV. Time domain measurement setup and procedure

Reflective delay lines have been described in the time domain with echoes delayed by durations determined by twice the distance from IDT to mirror divided by the acoustic velocity. Hence, the slower the wave, e.g. due to mass loading, the longer the delay introduced by the wave propagating on the surface of the gravimetric sensor. However, although the sensors are designed for compatibility with pulsed-mode time-domain Ground Penetrating RADAR (GPR) measurement compatible with fine time of flight delay measurement [6], laboratory measurements are performed in the frequency domain using a vector network analyzer (VNA) whose measurements are interpreted in the time domain through an inverse Fourier transform. Care must be taken, when performing phase analysis in the time domain, to match the Fourier coefficient organization of the numerical simulation software: under Matlab, GNU Octave or Numerical Python `numpy`, the convention is for the frequency to span from 0 to the sampling rate with the Nyquist frequency at half the sampling rate located in the middle of the abscissa range. On the opposite, a VNA measurement ranges from the center frequency minus half the span to center frequency plus half the span, so that the baseband center frequency is at the center of the abscissa range spanning from minus half the sampling frequency to half the sampling frequency. Since the discrete time Fourier transform is periodic, switching between conventions is only a matter of switching the quadrants from minus Nyquist frequency to 0 and 0 to Nyquist frequency as provided by the `fftshift()` command in all mentioned languages. Hence, after measuring the frequency f dependent scattering reflection coefficient $S_{11}(f)$, the time t domain characteristics $S_{11}(t)$ is computed as

$$S_{11}(t) = \text{ifft}(\text{fftshift}(S_{11}(f))) \tag{1}$$

and the phase of this quantity *at a fixed delay* determined as the reflected magnitude maximum is observed. The phase at fixed delay analysis is emphasized since it leads to a phase drop as the velocity decreases due to mass loading.

Indeed, the phase φ introduced by a wave at frequency f propagating at velocity v over a length D is $\varphi(f) = 2\pi f\tau = 2\pi f D/v$ but the latter expression emphasizes the phase *increase* as the velocity drops at *fixed frequency* (on the VNA output). However, in the time domain output at the measurement delay τ fixed as the inverse Fourier transform (ifft) bin, the phase at swept frequency f is expressed as $\varphi(\tau) = 2\pi\frac{v}{\lambda}\tau$ with λ the fixed wavelength determined by the IDT geometry. This expression leads to a *decreasing* phase at fixed delay τ as the velocity v *decreases*. Indeed all measurements displayed thereafter will exhibit decreasing phase at fixed delay indicative of mass loading with an acoustic wave velocity decreasing when the targeted analyte absorbs in the sensing surface.

V. Experimental results

One of the experimental challenges initially met when fabricating and measuring transmission and reflective LTO delay lines has been a notch in the frequency domain transmission sinc shaped transfer function in the former case or in the time-domain echoes in the latter case. These notches are attributed to the pseudo-shear wave generated on the LTO substrate where the surface wave guided on the surface by the guiding thin film if converted to a Love mode or metalization between

IDT and echoes to slow down the wave and confine it to the substrate surface, is accompanied with a bulk wave radiating towards the opposite flat side of the device. Since the wavevector along the propagation direction is the same for the surface and bulk wave, these two waves end up interfering on the reception IDTs, creating an interference pattern with notches where phases induces destructive summation of the vectors. This effect has been cancelled by mechanically depolishing the backside of the substrates on which the devices had been patterned, removing the notch in the transfer function (Fig. 3).

As a demonstration of the usability of the proposed device, a LTO reflective delay line with no specific surface functionalizion has been exposed to proteins from dehydrated milk in deionized water. The objective of the experiment is to assess the ability to recover the phase from multiple echoes of the reflective delay line under non-specific physisorption of immunoglobins as would be done classically for saturating the free areas of a functionalized biosensor surface. Fig. 5

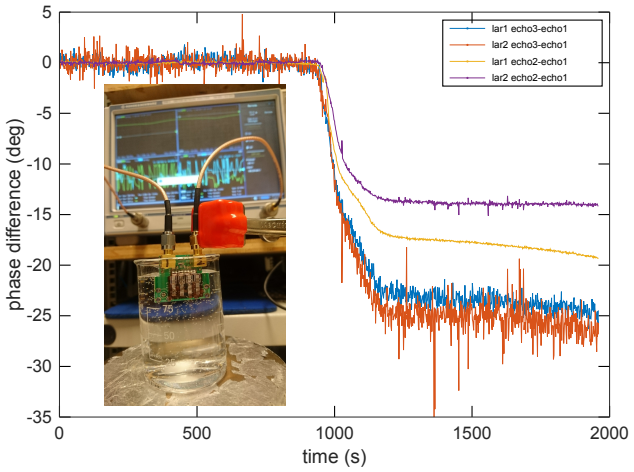

Fig. 5. Response of the four echoes patterned on a reflective SAW delay line upon exposure to a high concentration of immunoglobins from dehydrated milk in deionized water injected a 1000 s. Inset: picture of the experiment, emphasizing the lack of dedicated microfluidic handling elements on the acoustic path.

The various echoes i at delays τ_i ranging from 0.8 to 3.2 μs exhibit a phase shift φ_i proportional to the adsorbed mass and their respective absolute delay since $\varphi_i = 2\pi f \tau_i = 2\pi \frac{v}{\lambda} \tau_i \propto v \times i$ with $f = 200$ MHz the center frequency of the IDTs, and $\tau_i = d_i/c$ with d_i the two-way trip from IDT to echo length and c the acoustic velocity, varying upon exposure to the analyte to be detected.

Considering that a typical gravimetric sensitivity $S = \frac{df}{f} \cdot \frac{A}{dm} = \frac{d\varphi}{\varphi} \cdot \frac{A}{dm}$ relating the relative frequency variation $\frac{df}{f}$ or relative phase variation $\frac{d\varphi}{\varphi}$ when exposing a Love mode device operating at $f = 200$ MHz to a mass surface density $\frac{dm}{A}$ is in the 150 cm^2/g range, the measurement in Fig. 5 is analyzed as follows:

1) the shortest echo at at delay of 0.8 μs induces at the center frequency of 200 MHz a phase rotation of $\varphi = 360 \times 0.8 \times 200 = 57600°$,
2) the observed phase rotation of about 15° is interpreted as mass loading by an adsorbed protein thin film with mass density $\frac{dm}{A} = \frac{1}{S} \times \frac{[}{d}\varphi]\varphi \simeq 1.7$ μg/cm^2, a reasonable estimate for a non specific binding in a saturated dehydrated milk solution dissolved in phosphate buffer solution (PBS).

Considering a protein film as a polymer thin film with typical density in the 1.5 g/cm^3 range, this layer characteristics is interpreted as a $1.7/1.5 = 1.1$ μm thin adsorbed film, well within the thicknesses range investigated in Figs. 1 and 2 when considering the guiding properties of the thin film to convert the shear wave to a Love mode.

Considering that a VNA will allow measuring the phase with sub-° accuracy and that the differential measurement of subtracting the phase of multiple echoes [7] will allow for cancelling correlated effects such as range to the reader electronics (common to all echo delay measurements) and temperature or hydrostatic pressure, then a $d\varphi = 1°$ phase measurement resolution leads to a detection limit at $S = 150$ cm^2/g of $\frac{dm}{A} = 115$ ng/cm^2.

VI. Conclusion

Transmission and reflective delay lines on lithium tantalate have been designed to overcome the challenges of capacitive coupling of interdigitated electrodes exposed to high permittivity water with the surrounding medium inducing excessive insertion losses in the acoustic response. The resulting designs, propagating a pseudo-shear wave and compatible with energy confinement to the surface when guided in a thin polymer film acting as Love mode conversion layer, are shown to be compatible with measurement in liquid phase even at high ionic concentration (phosphate buffer saline solution) with no dedicated microfluidic system designed to prevent the liquid from reaching critical parts of the surface acoustic wave transducer as needed for low permittivity substrates.

References

[1] L. El Fissi, J.-M. Friedt, F. Cherioux, V. Luzet, and S. Ballandras, "Fabrication and packaging technologies of love-wave-based microbalance for fluid analysis," *Sensors and Actuators A: Physical*, vol. 162, no. 2, pp. 304–309, 2010.

[2] K. Mitsakakis, A. Tserepi, and E. Gizeli, "Integration of microfluidics with a love wave sensor for the fabrication of a multisample analytical microdevice," *Journal of microelectromechanical systems*, vol. 17, no. 4, pp. 1010–1019, 2008.

[3] A. Samarentsis, A. Pantazis, A. Tsortos, J.-M. Friedt, and E. Gizeli, "Hybrid sensor device for simultaneous surface plasmon resonance and surface acoustic wave measurements," *Sensors*, vol. 20, no. 21, p. 6177, 2020.

[4] F. Bender, R. Mohler, A. Ricco, and F. Josse, "Analysis of binary mixtures of aqueous aromatic hydrocarbons with low-phase-noise shear-horizontal surface acoustic wave sensors using multielectrode transducer designs," *Analytical Chemistry*, vol. 86, no. 22, pp. 11 464–11 471, 2014.

[5] J.-M. Friedt, G. Martin, G. Goavec-Merou, D. Rabus, S. Alzuaga, L. Arapan, M. Sagnard, and E. Carry, "Acoustic transducers as passive cooperative targets for wireless sensing the sub-surface world: challenges of probing with ground penetrating radar," *MDPI Sensors*, vol. 18, no. 1, p. 246, January 2018.

[6] D. Rabus, L. Arapan, P. Tanguy, J.-M. Friedt, and F. Chérioux, "Sampling frequency fluctuations of the Sensors & Software SPIDAR GPR when probing passive surface aoustic wave delay lines for pollution sensing," *IEEE Geoscience and Remote Sensing Letters*, 2020.

[7] A. Kang, C. Zhang, X. Ji, T. Han, R. Li, and X. Li, "SAW-RFID enabled temperature sensor," *Sensors and Actuators A*, vol. 201, pp. 105–113, 2013.